Medical Engineering and Physics 117 (2023) 103998

Contents lists available at ScienceDirect

Medical Engineering and Physics

journal homepage: www.elsevier.com/locate/medengphy

Fluid-structure interaction study of hemodynamics and its biomechanical influence on carotid artery atherosclerotic plaque deposits

Ayodele James Oyejide [a], Adetokunbo Andrew Awonusi [b], Olubunmi Ebenezer Ige [a,c,*]

[a] Department of Biomedical Engineering, Afe Babalola University, Ado-Ekiti 360231, Nigeria
[b] Department of Mechanical Engineering, University of Ibadan, Ibadan 200005, Nigeria
[c] Department of Mechanical Engineering, Rochester Institute of Technology, NY 14623, USA

ARTICLE INFO

Keywords:
Atherosclerosis
Cardiovascular
Carotid artery
Fluid-structure interaction
Hemodynamics

ABSTRACT

Atherosclerotic plaque deposits are common causes of blood flow disruption in the carotid artery bifurcation and the associated fluid mechanics has been extensively studied using Computational Fluid Dynamics (CFD) and Fluid Structure Interaction (FSI). However, the elastic responses of plaques to hemodynamics in the carotid artery bifurcation has not been deeply studied using either of the above-mentioned numerical techniques. In this study, a two-way FSI study was coupled with CFD technique, using Arbitrary-Lagrangian-Eulerian method, to study the biomechanics of blood flow on nonlinear and hyperelastic calcified plaque deposits in a realistic geometry of the carotid sinus. FSI parameters such as total mesh displacement and von Misses stress on the plaque, as well as flow velocity and blood pressure around the plaques, were analyzed and compared to variables such as velocity streamline, pressure and wall shear stress obtained from CFD simulation in a healthy model. The blood flow simulations reveal complete reversed blood flow behavior in the internal carotid artery, ICAs and external carotid artery, ECAs for both cases. In particular, this study suggests that plaques, irrespective of the masses, possess a high yielding response to hemodynamic forces at the attaching edges, while the surfaces are vulnerable to rupture.

1. Introduction

Approximately 600–700 mL of blood flow through the carotid arteries and into the human brain every minute to sustain the organ's vital functions [1]. However, this transport mechanism in the carotid arteries is sometimes altered by atherosclerosis, a medical condition characterized by build-up plaques. Plaques form when cholesterol, calcium, fibrous tissue, and other cellular debris accumulate at microscopic injury sites within the artery, which narrows and hardens the artery wall [2]. Under this condition, the rheological behavior of the blood is influenced, and supply of oxygen-rich blood to the brain is limited especially when the narrowing is greater than 70% [3]. At this stage, a patient is likely to develop symptoms of stroke, which is the most common disorder associated with carotid artery diseases and the third leading cause of death across the world [2,4].

Several studies have been carried out at cellular and molecular levels to understand the progression and role of atherosclerosis on blood hemodynamic in carotid artery bifurcation, as well as other biomechanical behavior of biological tissues [5–9]. However, most of these studies require human subjects and may come with some risks [10]. Consequently, researchers have taken advantage of available numerical biomechanics techniques, such as mathematical methods [11–15] and computational fluid dynamics (CFD) that saves time, provides high precision, and involves no use of biological samples to study flow behavior in humans [16,17]. This concept has predominantly been in use for decades, and one key assumption with the use of CFD is that the flow medium is rigid, with no slip at the walls [18–22]. This assumption is sufficient to estimate some computational variables, particularly when interested in the flow characteristics alone [23,24]. In biological vessels, however, especially when considering the velocity of flow, the tissues and organs are not that rigid; they interact with the fluid; a scenario described as Fluid-structure Interaction (FSI). The FSI technique is currently considered to give more realistic results because it accounts for the elastic behavior of biological vessels during simulation. For instance, to determine the arterial deformation of a typical carotid artery, Lee et al. [10] simulated the hemodynamic of the carotid artery using FSI. The technique reveals that geometric factors set for flow conditions do have significant influence on the hemodynamic

* Corresponding author at: Department of Mechanical Engineering, Rochester Institute of Technology, NY-14623 USA.
E-mail address: Ebenezer.Ige@rit.edu (O.E. Ige).

https://doi.org/10.1016/j.medengphy.2023.103998
Received 21 January 2023; Received in revised form 16 May 2023; Accepted 18 May 2023
Available online 20 May 2023

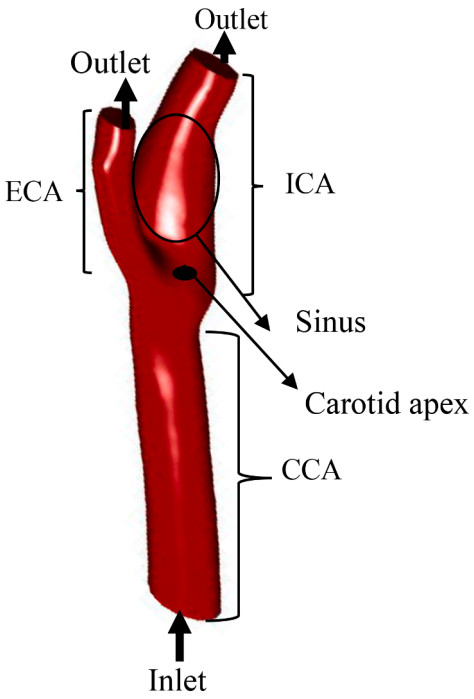

Fig. 1. Schematic descriptions of carotid artery model and blood flow path. ICA (supplies blood to both the brain and eyes), ECA (supplies the throat, face, mouth, and similar structures).

characteristics of the carotid artery. Chiastra et al. [24] also studied hemodynamic of stented coronary artery through fluid–structure interaction. Their result indicates that the rigid-wall assumption for fluid dynamic simulations will only be adequate if the aim of the study is the analysis of near-wall quantities like wall shear stress, but FSI may be closely accurate for other quantities. Sousa et al. [25] evaluated healthy blood flow in vascular geometries constructed from Doppler ultrasound images of carotid artery bifurcation by modeling both rigid and compliant walls. Simulation results indicate that velocity and WSS distributions are similar and FSI model presents larger recirculation area and lower maximum WSS value. Zouggari et al. [26] also developed models of healthy and stenosed carotid arteries to examine how wall shear stress is influenced by the formation of plaques. Both CFD and FSI were used to investigate the carotid wall deformation, and FSI shows that the plaque reduces the wall shear stress in the region after it and creates areas of recirculation.

In a study by Lopes et al. [27], they evaluated blood flow in rigid and elastic models of carotid artery walls using patient-specific geometry. The study, which involves typical computational fluid dynamics in the rigid model and FSI study in the elastic model, shows that atherosclerosis is more likely to occur in the carotid sinus region, due to its low values of Time-Averaged wall shear stress, when considering the mechanical properties of the artery in this area. In a study by Bantwal et al. [28], the authors constructed a plaque in the sinus region leading to lumen stenosis artery and hemodynamic parameters such as Oscillatory Shear Index (OSI), and Relative Residence Time (RRT); a marker of disturbed blood flow, were analyzed and compared to established data in healthy arteries. The gotten FSI parameter indicated high OSI and RRT, a condition for potential thrombus formation at the carotid sinus in case of plaque rupture. In a more recent study attempting to analyze the nonlinear dynamics of atherosclerosis in carotid artery bifurcation, Pillai et al. [18] performed FSI simulations that suggest that the technique has the potential to be used as a tool to forecast the onset of stroke and brain ischemia. Nevertheless, most FSI studies of the carotid artery bifurcation have accounted for elastic arterial walls, but the mechanics of plaque response to hemodynamics on such vessels, and vice versa, has not been deeply studied.

Table 1
Healthy carotid artery geometry.

Section	Diameter (mm)	Area (m^2)	Approximate length (mm)
CCA	6.30	31.72	32.12
ICA	4.50	15.90	21.79
ECA	3.00	7.07	19.16
Sinus	6.75	35.78	14.53

Although the fluid structure interaction behavior of blood flow around plaque deposits in the human arteries has been reported in a number of articles, such numerical models and simulations have concentrated on the elasticity of the arteries during blood motion, with no significant report about the simultaneous elastic behavior of the artery and the plaque deposits to the blood flow. We accounted for this gap by incorporating both solid and fluid mechanics numerical methods to formulate realistic and responsive interaction between pulsatile blood flow and elastic models of plaque deposits attached to the sinus of a carotid artery. In the methodology, we described the CAD modeling of the plaques, the numerical modeling of the blood, the boundary conditions and the CFD and FSI numerical models implemented in solving the flow physics. In the subsequent sessions, outcomes of CFD and FSI simulations in both geometries, for the flow velocity, blood pressure, wall shear stress, plaque displacement and Von Misses stress on the plaques, were presented, compared and discussed.

2. Methods

2.1. Geometry modeling

Herein, we replicated the simplified realistic carotid artery geometry developed in [27], for the healthy case, shown in Fig. 1. Parameters employed in developing this geometry are presented in Table 1. In the second geometry, we imposed significant lumen reduction (in form of plaques) of within 85–90% at the sinus (ICA), while ECA and CCA have no stenosis (see Fig. 2). To incorporate the plaque deposits and account for their elastic properties, the geometry and fluid domain was developed on the Mechanical system of the Ansys software. Upstream in both models is the common carotid artery, referred to as the CCA. Just before the bifurcating branches is the carotid apex, which is followed downstream by the internal carotid artery, ICA, supplying blood to the brain and the external carotid artery, ECA, supplying the face and neck regions (see description in Fig. 1). Recent studies have reported that the carotid sinus is a favorable location for plaque progression because of the temporal disturbances experienced in its environment; a justification for building the plaques in the sinus [27,28]. Regarding the properties of the plaques, idealistic calcified plaques of varying sizes were used, fixed at opposing directions (about 0.23 mm apart) on the arterial wall in the sinus. The plaque geometry parameters are presented in Table 2 and Fig. 2, respectively.

2.2. Numerical modeling of plaques

The plaques in the sinus were modeled as a nonlinear and hyperelastic material [29] with strain energy function of Yeoh third order material model, expressed mathematically in Eq. (1), with a Poisson's ratio of 0.49 [30].

$$W = c_{10}(I-3) + c_{20}(I-3)^2 + c_{30}(I-3)^3 \quad (1)$$

The c_{10}, c_{20},and c_{30} are the material constants with values selected from experiment data of [29] gotten for the heavily calcified plaque of stenosed femoral artery. The I represent strain invariant while c_{10} = 46.2 kPa c_{20} = − 14.7kPa, and c_{30}= 4.95 kPa.

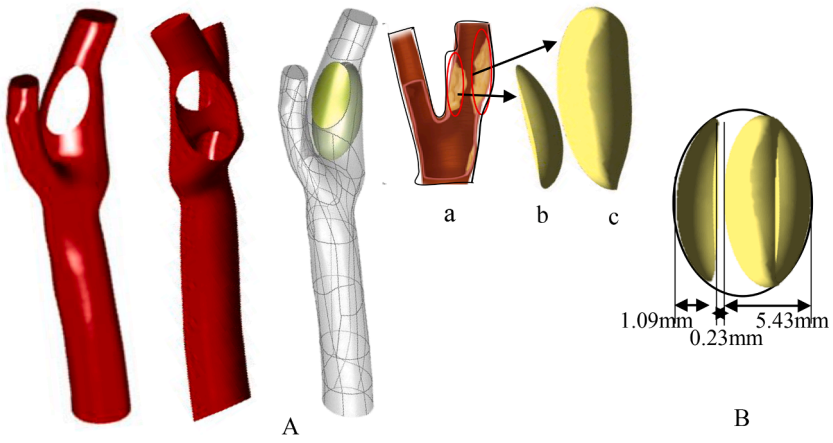

Fig. 2. (A) Unhealthy coronary artery showing model with extracted and fixed plaques. (B) Cross-sectional view of the sinus showing the plaque orientation, distance apart, and distance away from the wall.

Table 2
Plaque geometry parameter.

Surface Area	Smaller Plaque	Lager Plaque
Surface Area (mm^2)	72.9	198.5
Volume (mm^3)	32.6	195.6
Distance from wall (mm)	1.09	5.43
Density (kg/m^3)	1450	1450
Material	nonlinear and hyper-elastic material	

Table 3
Mesh sensitivity study.

Element size (mm)	Total No. of Elements	Average inlet pressure (Pa)	Average outlet velocity (m/s)
3	88,085	13,432	0.235
2.5	88,443	13,438	0.244
2.0	89,152	13,443	0.254
1.8	89,582	13,444	0.257
1.6	90,582	13,446	0.261
1.4	91,722	13,447	0.261
1.2	93,947	13,448	0.259

2.3. Modelling of blood rheology

Realistically, blood is a non-Newtonian incompressible fluid with pulsatile velocity. The non-Newtonian and incompressible components are generally accounted for by the continuity and Navier-Stokes equations represented by Eqs. (2) and (3):

$$\nabla . v = 0 \tag{2}$$

$$\rho(\partial v / \partial t + v.\nabla v) = -\nabla p + \mu \nabla^2 v + f \tag{3}$$

To account for the realistic physiological blood shear-thinning behavior, the Carreau viscosity model was employed. This model is mostly used and recommended by previous literature on hemodynamics [31]. The mathematical variables for this model are represented in Eq. (4) as:

$$\mu = \mu_\infty + (\mu_0 - \mu_\infty)\left[1 + (\lambda\gamma)^2\right]^{(n-1)/2} \tag{4}$$

Where, infinity shear viscosity; $\mu_\infty = 0.00345$ Kg/m^{-2}, zero shear viscosity; $\mu_0 = 0.056$ Kg/m^{-2}, time constant; $\lambda = 3.313$ s, power law index; $n = 0.3568$, and γ is the strain rate, at blood constant density of 1060 kg/m^3.

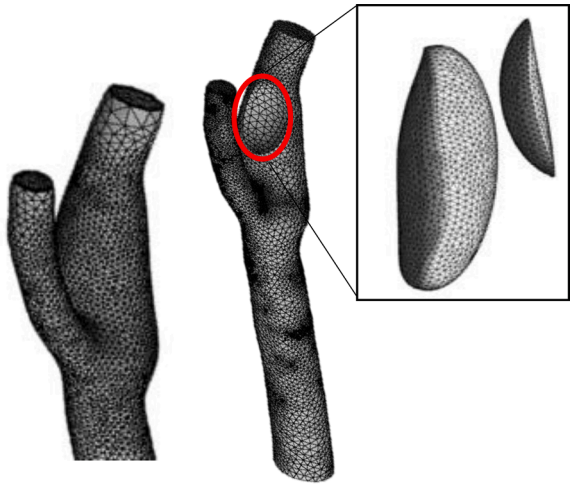

Fig. 3. The selected mesh setting of the model.

2.4. Mesh consideration

Mesh sensitivity study (see Table 3) was conducted on the healthy carotid artery bifurcation to offer a solution-independent element size. An inflation of 5 layers with a maximum thickness of 0.6 mm was included in the mesh settings, while a constant local element size of 0.5 mm was set at the bifurcation region to ensure that the stimulated results were independent of the mesh settings. Thereafter, mesh sensitivity study was conducted for the element size set for the remaining region of the artery, and a suitable element size of 1.6 mm was selected after the study. Data from the mesh study is presented in Table 3. Regarding the plaques, tetrahedra mesh of 46,266 elements with minimum orthogonal quality of 0.235 and maximum skewness of 0.764 was used, while the selected mesh settings in the healthy models was applied to the flow component in the model.

Given that the accuracy of a simulation is influenced by the number of elements in the grid, a mesh sensitivity study was conducted on the healthy carotid artery to arrive at a suitable solution-independent grid size, from which a further increase in the element number does not produce significant differences in the results, and could cause increase in computational resources such as simulation duration. Table 3 and Fig. 4, show that an increase in the number of elements yields significant differences in the variables (average inlet pressure and outlet flow), but further increase in the grid size of 90,582 does not offers significant differences in both variables. Therefore, a grid size of 90,582 was

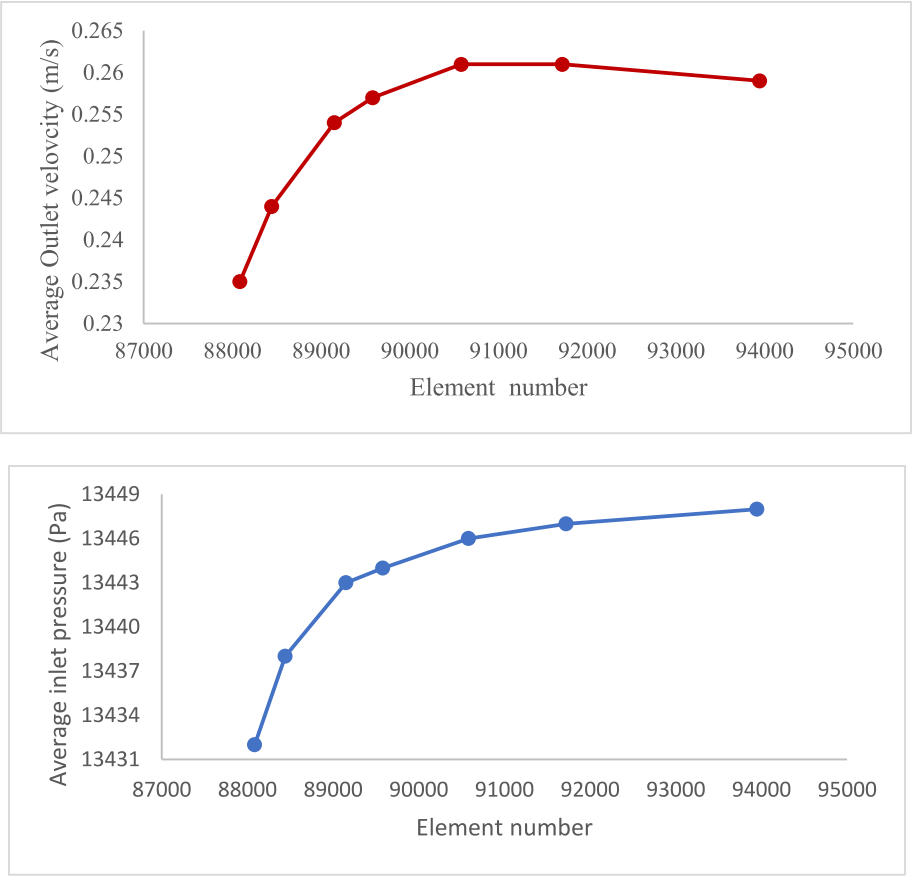

Fig.. 4. Variation of the velocity magnitude with mesh element size.

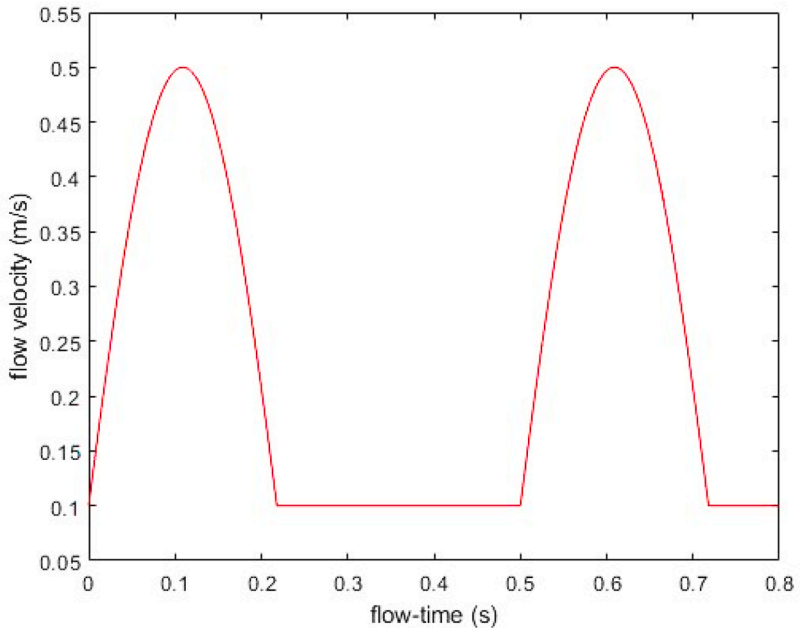

Fig. 5. Inlet velocity profile in the study, presented in a cyclic blood flow.

selected for the simulation.

2.5. Boundary conditions

The velocity of blood flow at the inlet is pulsatile, defined as a periodic function through user defined function (UDF), varying from 0.1 m/s during diastole to 0.5 m/s during contraction, depicted by the obtained waveform in Fig. 5 [32]. A uniform gage pressure of zero was assumed at the outlet with the assumption that the pressure downstream of the arteries is the same, though, ideally, physiological parameters can

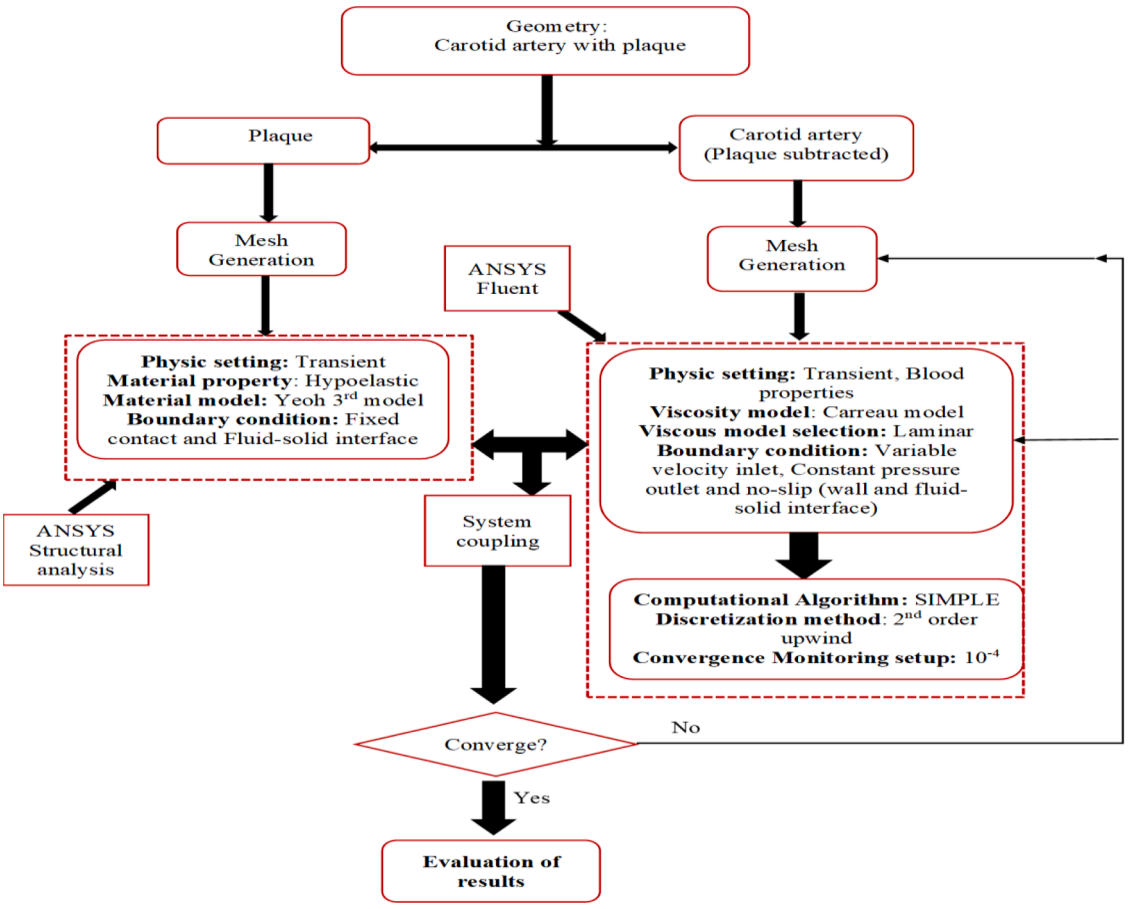

Fig. 6. Flow chart representation of the methods for numerical modeling and CFD-FSI coupling.

be fixed at the individual outlets in a more patient-specific geometry [33]. For the arterial geometries, a no-slip boundary condition was set to the wall of the artery, to save simulation time, though the plaques were assigned elastic properties, since it was our main focus.

2.6. Numerical modeling and solver for FSI and CFD

2.6.1. Fluid-structure interaction modeling

To evaluate the modification in the deformation on the plaques as the flow filed changes during the pulsating motion of the blood, two-way FSI was used, and the FSI simulations were performed using the Arbitrary-Lagrangian-Eulerian (ALE) method (expressed in Eq. (5) [34]). The fluid domain was also discretized with the finite volume method.

$$\rho f\left(\frac{\partial u}{\partial t}+((u-ug)\cdot\nabla)u\right)=-\nabla p+\mu\nabla^2 u \tag{5}$$

Where, ρf, p, u, and ug are the fluid density, the pressure, the fluid velocity, and the moving coordinate velocity, respectively. The term ($u - ug$), in the ALE formulation, is added to the conventional Navier-Stokes equations to account for the movement of the mesh. The displacement and equilibrium forces at the interface of the blood and plaques are represented by Eqs. (6) and (7) [34]:

$$uf,\Gamma = us,\Gamma \tag{6}$$

$$\overrightarrow{tf},\overrightarrow{\Gamma} = \overrightarrow{ts},\overrightarrow{\Gamma} \tag{7}$$

where uf, Γ is the displacement of the fluid at the interface, us, Γ, the displacement of the solid at the interface, $\overrightarrow{tf}$, $\overrightarrow{\Gamma}$, the forces of the fluid on the interface and $\overrightarrow{ts},\overrightarrow{\Gamma}$, the forces of the solid on the interface.

2.6.2. CFD-FSI coupling and solver

The blood and plaque domain were solved simultaneously with bidirectional data transfer between the fluid solver and mechanical solver. Pressure gotten from CFD was exported to interaction (exposing) surface of the plaques for structural analysis, and deformation information on the plaque is relayed back for flow (CFD) update and analysis at each time step. A system coupling was incorporated in the ANSYS Workbench to couple the mechanical solver (transient structural analysis) and fluid flow solver (Fluent). We selected a "fixed support" boundary condition in the mechanical solver (a solid mechanics aspect of the boundary conditions), to restrict rotation and displacement at the interface between the plaque deposit and the sinus wall of the carotid, during blood flow in the ICA. While, on the surface exposed to the blood flow, a condition of "fluid solid interface" was applied, that basically allows the solid to deform under the influence of the blood flow, and location where the bidirectional data transfer occur between the two solvers. The computational algorithm and discretization method are PISO algorithm [35,36] and Second Order Upwind, respectively, shown in Fig. 6, while the time step was set at 0.0016 s, with 50 iterations per step [37]. Similar parameters were adopted for CFD approach in the healthy carotid artery model, using the finite-volume discretization method and the SIMPLE computational algorithm, except the coupling method. It should be noted that the CFD simulations was conducted on only the healthy carotid to solve the velocity, wall shear stress and pressure variables.

3. Results and discussion

This section presents results for the 2-way FSI and CFD simulations. The results of interest in the unhealthy artery are primarily the blood

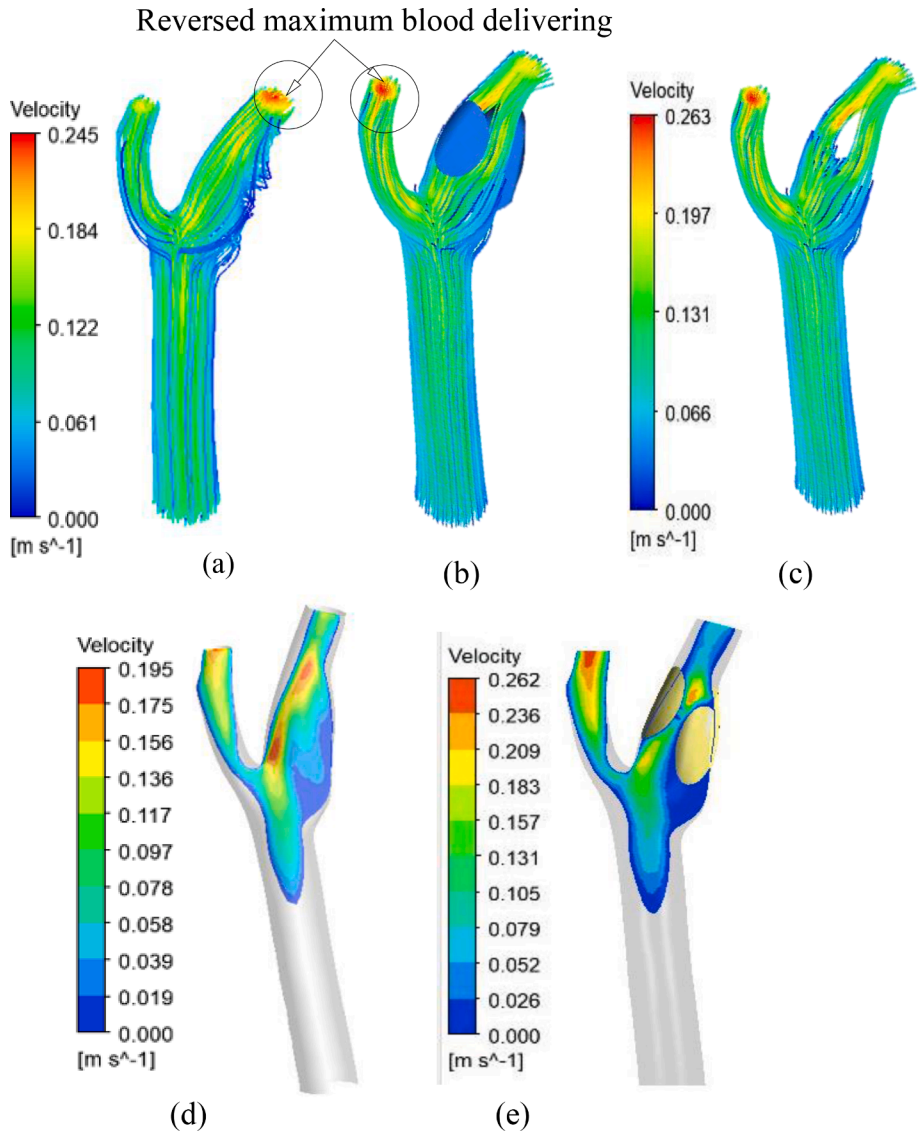

Fig. 7. Velocity streamline in (a) healthy (b) unhealthy with plaque and (c) unhealthy showing space occupied by the accumulated plaques (d) velocity contour in healthy and (e) velocity contour in the unhealthy carotid artery bifurcation models, respectively.

flow velocity along the plaque constriction, the entire plaque deformation, and the Von Miss stress which expresses the plaques yielding energy to rupture. We also presented the wall shear stress and blood pressure in both the healthy and unhealthy models.

3.1. Results

3.1.1. Velocity streamlines

The velocity streamlines for both the healthy and unhealthy carotid artery bifurcations are presented in Fig. 7a–c, respectively. In the healthy model, at systolic, blood flow in the CCA with regular vertical partitions, which was divided into eight (8) around the entire diameter. However, the regular flow pattern was disrupted at the carotid apex. Here, the flow partitions at the throat of the ICA expanded and split all the way to the sinus and the outlet. On the other hand, in the unhealthy carotid model, the blood flow appears to be steady, and a velocity of about 0.066–0.131 m/s was sufficient to drive blood from the inlet to the bifurcation. However, the flow velocity increased at the ICA and ECA, with a peak velocity magnitude of 0.263 m/s, seen at the outlet region of the ICA, into the face and neck. At the ICA where the plaques obstruct blood flow, velocity dropped at the base of the plaques to almost 0 m/s, before pathing way around the plaques towards the outlet, delivering blood into the brain. The result reveals significant information about the blood delivering capacity in both arteries. In the healthy carotid artery, rich blood flow was delivered into the brain at maximum speed of 0.245 m/s through the ICA. Whereas, in the unhealthy model, the drop in flow magnitude due to the plaques, led to weak blood delivering velocity, as low as 0.197 m/s, which is 5 times (0.048) lesser when compared to the healthy geometry. As a consequent of the obstruction and blood flow drop in the ICA of the unhealthy carotid model, pressure led to reserved blood flow that increases the flow velocity in the ECA (0.263 m/s), in this case, favoring blood supply into the face and neck region with a speed approximately 75% greater than the delivery speed into the brain (0.197 m/s).

3.1.2. Velocity contours

The velocity profiles are presented in Fig. 7d and e to buttresses the streamline results. To understand the blood flow rates around the plaque only, we obtained FSI simulation results for velocity of flow at specific regions; (a) at the plaque bases (carotid apex) (b) at mid-section and (c) at the top section (head) of the plaques. Overall, around the plaque region, velocity was highest at the head, followed by the mid-section and

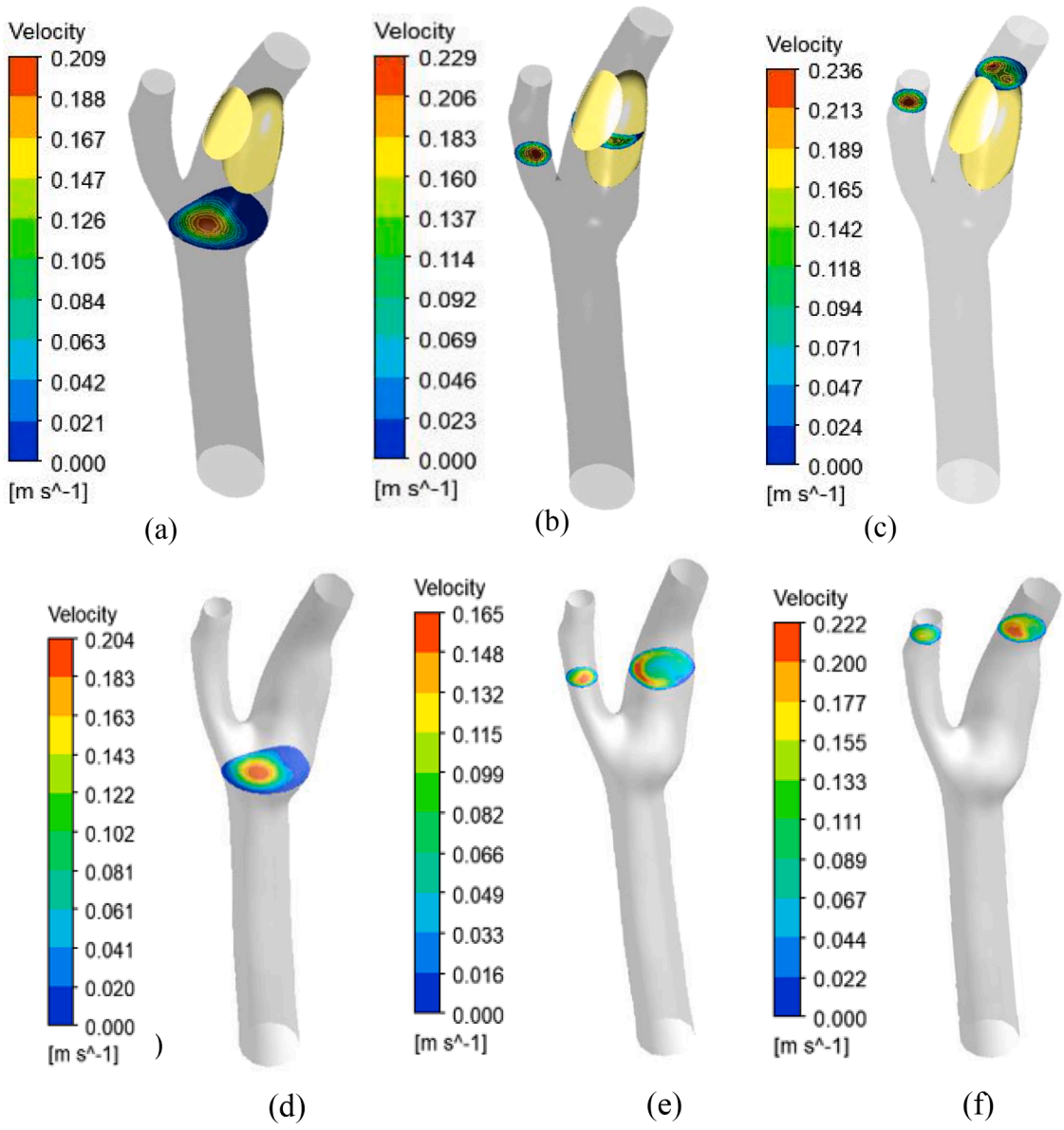

Fig. 8. Blood flow rate at (a, d) the bases (b, e) at mid-section and (c, f) at the top section (head) of the plaque in unhealthy and healthy carotid artery bifurcations using FSI and CFD, respectively.

then at the apex. Perhaps, the velocity distribution is affected by the magnitude and orientation of the plaques. Placing the large plaque deposit at the base of the sinus induced high pressure on the flow, capable of almost stopping the flow on first encounter. Nonetheless, after what can be described as a brief flow delay at the plaque obstruction, the blood gained a little momentum to move up into the outlet region as it attained a relatively high velocity in the ICA, into the brain.

3.1.3. CFD and FSI evaluation of hemodynamics at the plaque sections

An attempt was made to compare the velocity characteristic in the healthy carotid model (see Fig. 8d–f), at the exact section of plaque accumulation in the unhealthy model, using CFD. Here, we realized that the maximum velocity at the sinus head was 0.22 m/s, which tends to develop towards the left side of the arterial wall. The next peak velocity was found at the carotid apex, with flow velocity of 0.204 m/s, concentrating at the center as found in the unhealthy mode. The lowest flow velocity was found at the sinus mid-section with a half-moon shape and velocity magnitude of 0.165 m/s. The tiny half-moon flow was also seen developing on the left side of the artery wall, in the sinus, due to the relatively regular shape compared to the right side with the huge area curvature. In general, both the overall velocity contour and blood flow rate at the three selected sections, indicate extreme velocity magnitude in the external carotid artery, ECA, which suggests the possibility of high wall shear stress (WSS) in this carotid branch.

3.1.4. Displacement

Depending on the plaque buildup and flow velocity, the blood flow across the plaque surfaces should yield some responses. Such reaction or response of solids to fluid passage are mostly referred to as Total Mesh Displacement (TMD) or deformation, shown in Fig. 9A. Here, three distinct results were obtained.

First, at the back of the plaques where they are attached to the internal arterial wall, the fluid passage had no displacement effect, indicating that the plaques plugged tightly to that region. Second, the flow had less displacement effect on the surface of the smaller plaque deposit when compared to the larger one. The plaques properties seem to play a huge role in this case. Ordinarily, the smaller plaque should display the highest displacement effect since it has the smaller surface area.

		Complete model view	Plaque isolated view
A	**Total mesh displacement** (Plaque deformation)	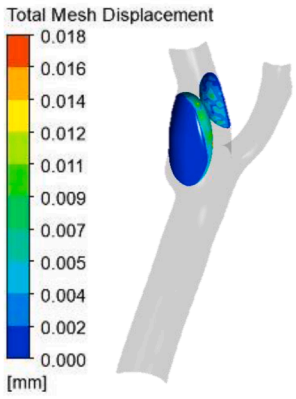	
B	**Von Miss Stress** (Plaque yielding energy to rupture)	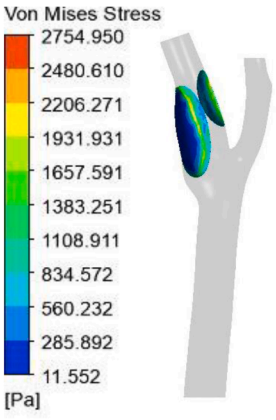	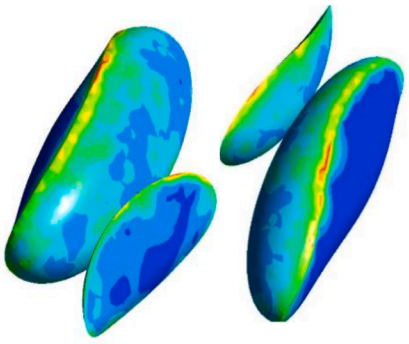
C	**Wall shear stress (WSS)**	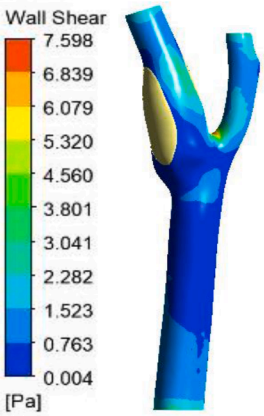	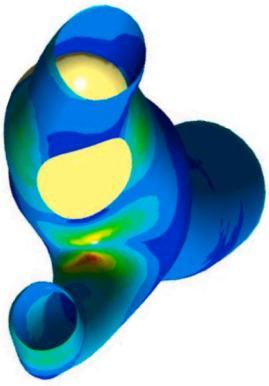

Fig. 9. Results of FSI simulations on the plaques responses to the blood hemodynamics in term of (a) total deformation (b) rupture and (c) arterial wall shear stress.

However, in this case, both plaques have same density of 1450 kg/m^3, and the surface geometry of the smaller plaque encourages slippery transition of blood along the constriction. By considering the velocity profile in Fig. 7, the orientation causes high flow drag on the right of the sinus where the bigger plaque was placed, causing maximum displacement at this site over a large surface area of 198.5 mm^2 compared to 72.9 mm^2 in the smaller plaque. Third, despite the low velocity at the constriction, the flow pulled tiny portions of the plagues, displacing them up to 0.012 mm from the original position. It is also worth noting that the greatest deformation occurred towards the center of the plaques, which increases as the narrowing increased (see Fig. 9A).

3.1.5. von Mises stress on the plaque

The rupture of atherosclerotic plaques is known to be associated with stresses that act on or within the arterial wall, leading to issues such as thrombus formation and progression of the atherosclerotic lesion [25]. On like the total mesh deformation, the von Mises stress on the plaque reveals that the blood motion exerts considerable stresses on notable portion of the plaques. As shown in Fig. 9B, the blood motion exerted forces on the edges, the external surfaces and the attaching surfaces of the plaques. However, the least stress occurred at the regions where the plaques attached to the internal arteria wall. The stress in this attaching region is higher on the smaller plaque deposit at 834. 572 Pa compared with the bigger deposit where maximum stress is between 285.892 and 560.232 Pa. In addition, the plaque edges, in both cases, appears to be

Table 4
Comparison of hemodynamic properties in both healthy and unhealthy carotid branches.

	Healthy Carotid Model (CFD)			Unhealthy Carotid Model (FSI)		
Maximum	CCA	ICA	ECA	CCA	ICA	ECA
Vel. (m/s)	0.204	0.222	0.165	0.209	0.229	0.236
Wall Pre. (Pa)	13,382	13,367	13,358	13,404	13,382	13,361
Blood Pre. (Pa)	13,363	13,368	13,353	13,380	13,374	13,356
WSS (Pa)	3.727	1.871	1.406	2.282	2.282	3.041

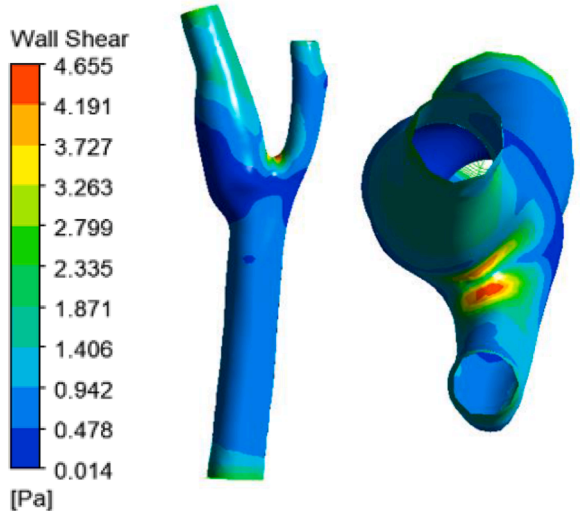

Fig. 10. Wall shear stress in the healthy carotid artery bifurcation model.

more vulnerable to rupture. On the surfaces, the stresses appear to act equally on both plaque sizes, except that there were a few contours on the bigger deposit, which could indicate cracking. However, the cracking does not seem to be heavy enough to cause surface rupture of the plaque deposits.

3.1.6. Wall shear stress

An essential parameter in estimating the rate of arterial wall degeneration is the wall shear stress. In this session, we discuss the corresponding relationship between flow pressure and velocity (obtained from both FSI and CFD), which are important computational variables when evaluating WSS. As expected, in both carotid geometries, minimal WSS was present at the CCA due to its relatively linear passage. However, at the bifurcation in both models, just before blood flows into the internal and external branches, the WSS increased significantly. In the unhealthy carotid model, and just around the vicinity of the plaques, WSS increased to a maximum value of 7.598 Pa (see Fig. 9C). Due to the reverse flow that led to increased blood flow in the ECA in this case, high WSS was seen in the branch, as high as 3.041 Pa particularly at the exit point. When compared to the CFD result for the healthy model, where maximum velocity reaches 0.194 m/s at the ICA, the highest WSS were realized at the bifurcation, the ICA (particularly the sinus) and the ECA, respectively. To a large extent, the WSS distribution in the healthy carotid artery is safe as it is directly proportional to the magnitude of the inlet blood velocity. Table 4 and Figure shows a comparison between values of WSS gotten at the CCA, ICA and ECA in both carotid models.

3.1.7. Blood pressure

It is important to study the influence of the plaque accumulation in the sinus on the arterial blood pressure to predict associated health implications. Pressure distribution on both walls of the healthy and unhealthy carotid artery models was similar, especially at the CCA and ECA as presented in Fig. 11a-b. The maximum wall pressure was seen at the entrance in the CCA with magnitudes of 13,382 Pa and 13,404 Pa for the healthy and unhealthy models, respectively. The wall pressure dropped gradually upstream the bifurcation and the lowest drops were seen at the outlets of both the ICA and ECA in both models. Despite the similarities, the presence of the plaques influenced the blood pressure in the unhealthy carotid model as revealed by the FSI simulation. First, thick blood layer was found at the carotid apex with maximum value of 13,397 Pa, which is 24. 68 Pa greater in magnitude when compared to similar blood layer at the healthy carotid apex. In addition, the sinus pressure in the unhealthy carotid model was far higher than that of the healthy model. The plaques created a build-up of high blood flow pressure at the base of the sinus, which began approximately half-way upstream the common carotid artery. Also, in between the plaques, at the closest constriction to blood flow, a fluctuation was observed in the blood pressure magnitude, where the pressure dropped from 13,368 Pa to 13,350 Pa and finally to 13,344 Pa, before dropping completely to 13,332 Pa at the exit, as shown in Fig. 11d. Unlike in the unhealthy model, blood pressure was relatively steady in the healthy model (see Fig. 11c) with the highest-pressure magnitudes seen in the CCA (up to the ICA base), at the bifurcation, and on both ends of the sinus wall. A general observation about the blood pressure in the healthy carotid model is that, even in the absence of plaques, blood pressure is higher in the internal carotid artery, particularly in the sinus, compared to the external carotid artery.

3.2. Discussion

From the results in Fig. 7, in the healthy model, the regular vertical partitions in the CCA at systolic suggest that the blood flow is streamlined and regular, which is characteristic of healthy blood flow. However, disruption of the regular flow pattern occurs at the carotid apex where the flow partitions at the throat of the ICA expand and split, possibly due to changes in the arterial wall and blood flow dynamics. These changes may be attributed to the geometry of the carotid bifurcation and the surrounding vasculature. Such changes can affect the biomechanics of the arterial wall and the hemodynamics of the blood flow in the artery, which can have implications for the onset and progression of atherosclerosis [38]. In contrast, the unhealthy carotid model suggests that the blood flow is not streamlined and regular. The increase in velocity at the ICA and ECA, with a peak velocity magnitude of 0.263 m/s, seen at the outlet region of the ICA, into the face and neck, indicates the development of stenosis or narrowing of the arterial lumen, which is common in atherosclerosis. The flow velocity drop at the base of the plaques to almost 0 m/s at the ICA is a result of the obstruction of blood flow by the plaque, leading to reduced blood flow to the brain.

In Section 3.1.3, where we investigated the velocity characteristics and blood flow rate at different sections of both the healthy and unhealthy carotid artery model using both CFD and FSI simulations for comparison, the maximum velocity was found at the sinus head, which tends to develop towards the left side of the arterial wall. This peak velocity was also found in the unhealthy model, which is where plaque accumulation occurs. The next peak velocity was found at the carotid apex, which is also consistent with the unhealthy model. The results suggest that there is an extreme velocity magnitude in the external carotid artery (ECA), which could indicate the possibility of high wall shear stress (WSS) in this carotid branch, leading to the deformation of endothelial cells, inflammation and the formation of atherosclerotic plaques [39,40]. This information could help clinicians and researchers to better target these areas for intervention and treatment.

Furthermore, the result of the Total Mesh Displacement and Von Mises stress on the plaques, suggest that the properties of the plaque, such as its size, shape, and surface geometry, can play a significant role in the displacement effect. As observed in Fig. 9A and B, despite the low velocity at the constriction, the flow pulled tiny portions of the plaque, displacing them up to 0.012 mm from the original position, implying that even small changes in the flow conditions can cause deformation of

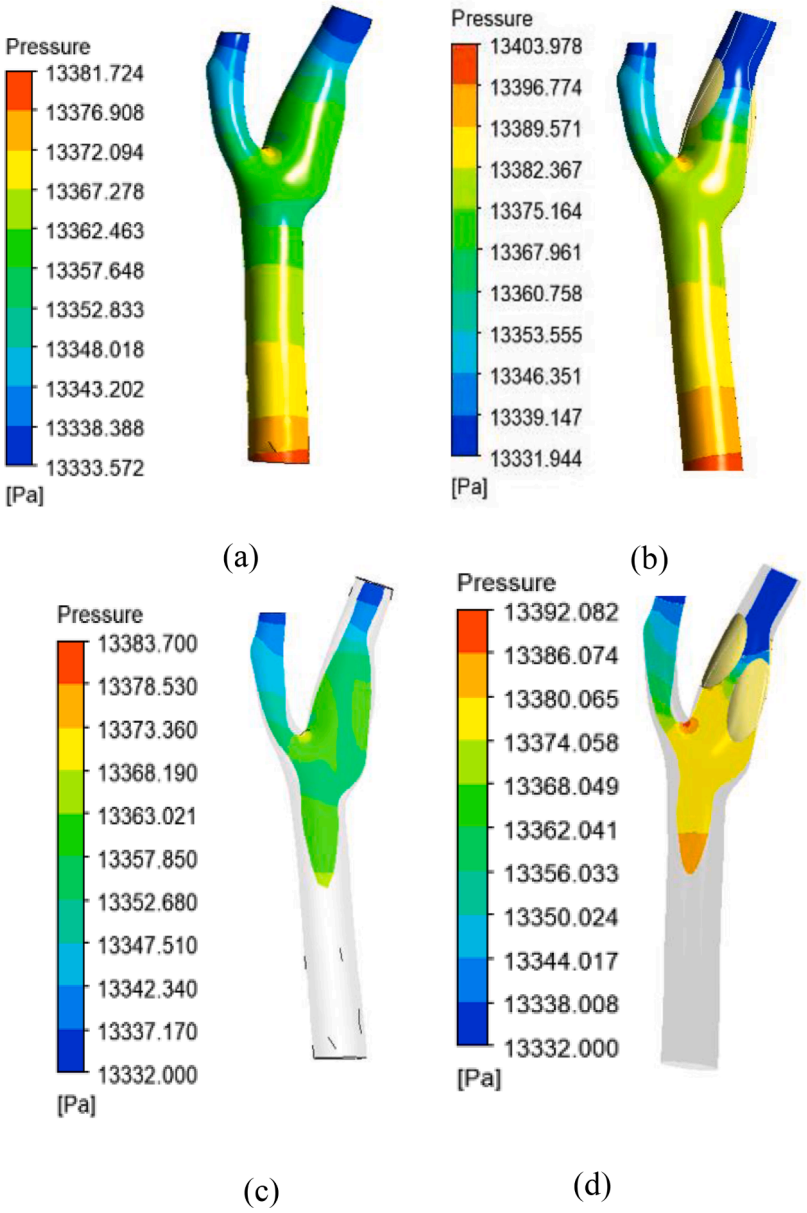

Fig. 11. Wall pressure distribution and blood pressure in (a, c) healthy and (b, d) unhealthy carotid bifurcation models, using CFD and FSI, respectively.

the plaque, which can have important implications for the development and progression of atherosclerosis. The von Mises stress is a measure of the stress state at a particular point in a material, and it is commonly used to assess the mechanical integrity of structures under load. The findings of this study reveal that the von Mises stress on the plaque is highest at the edges, indicating that these regions are more vulnerable to rupture. The results also indicate that the attaching region of the plaque to the internal arterial wall experiences higher stress in the case of the smaller plaque deposit. These findings have important implications for understanding the biomechanical influence of hemodynamics on atherosclerotic plaque development and rupture. The stresses acting on the plaque can lead to issues such as thrombus formation and progression of the atherosclerotic lesion [41] which can ultimately lead to the rupture of the plaque. Therefore, understanding the stresses acting on the plaque and their distribution is critical in developing effective strategies for the prevention and treatment of atherosclerotic plaque deposits.

Based on the results for the wall shear stress, we found that the WSS distribution in the healthy carotid artery is safe, as it is directly proportional to the magnitude of the inlet blood velocity. In other words, as long as the blood flow remains within a certain range of velocities, the WSS in a healthy carotid artery will not exceed safe levels. On the other hand, an increase in WSS is more pronounced in the unhealthy carotid model, particularly in the vicinity of the plaques, where WSS reaches a maximum value of 7.598 Pa. The high WSS could be associated with the reverse flow behavior at the plaque constriction, that led to increased blood flow in the external carotid artery (ECA), leading to higher WSS in the branch, as high as 3.041 Pa particularly at the exit point.

The result of the blood pressure, shown in Fig. 11a–d, highlights the importance of studying the influence of plaque accumulation in the carotid artery on arterial blood pressure to predict associated health implications. Although similar blood flow patterns were observed in FSI simulation of both healthy and unhealthy carotid artery models, the presence of plaques influenced the blood pressure in the unhealthy carotid model, with a thick blood layer found at the carotid apex with a maximum value of 13,397 Pa, which is 24.68 Pa greater in magnitude when compared to the similar blood layer at the healthy carotid apex.

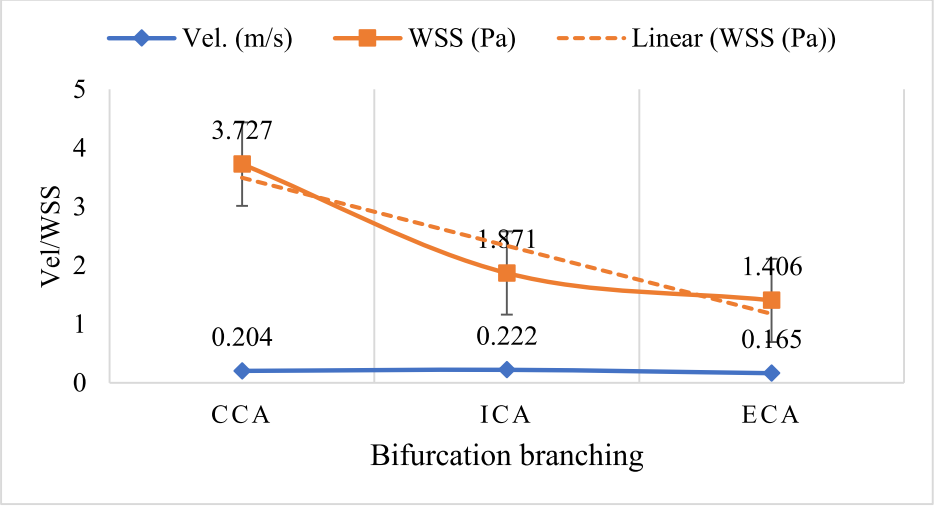

Fig. 12. Flow profile of direct relationship between velocity of flow and corresponding wall shear stress in all branches of the healthy carotid artery model (CCA, ICA and ECA) under study.

This indicates that plaque accumulation causes an increase in blood pressure in the unhealthy carotid model. In addition, in between the plaques, at the closest constriction to blood flow, a fluctuation was observed in the blood pressure magnitude, where the pressure dropped before dropping completely at the exit. This suggests that the presence of plaques creates an uneven flow of blood, causing turbulence and pressure drops. This turbulent flow can contribute to the formation and progression of atherosclerotic plaques, which is established by studies [42,43] to lead to a higher risk of cardiovascular disease.

The results of this study underscore the importance of studying the fluid-structure interaction in the carotid artery to understand the biomechanical influence of hemodynamics on atherosclerotic plaque deposits. FSI modeling allows for a more accurate representation of the interaction between blood flow and the arterial wall, which is essential in understanding the distribution of WSS in the carotid artery. Therefore, the findings of this study can be used to develop better strategies for preventing and treating atherosclerosis, such as optimizing blood flow patterns to reduce the risk of plaque formation and identifying patients at higher risk of developing atherosclerosis.

The main findings from the results are that: firstly, the stresses acting on the plaque are a result of the forces exerted by the blood flow on the plaque, and the response of the plaque to these forces is a complex interplay of material properties, geometry, and fluid mechanics. Secondly, these results suggest that changes in hemodynamics and arterial wall biomechanics may contribute to the development of atherosclerotic plaques in the carotid artery.

4. Conclusion

In the present work, we examined the nature and implication of a simultaneous interaction between plaque deposit and blood flow in the sinus of a carotid artery, using CFD and 2-way transient fluid-structure interaction (FSI) technique, respectively. The methods are applied to two different realistic geometries of a healthy and atherosclerotic carotid artery bifurcations, with physiological pulsatile blood flow conditions. We infer from the study that:

- By accounting for the realistic properties of the plaques, the deposits are vulnerable to rupture at the surfaces and at the attaching edges on the internal arterial walls. Significant rupture effect will take

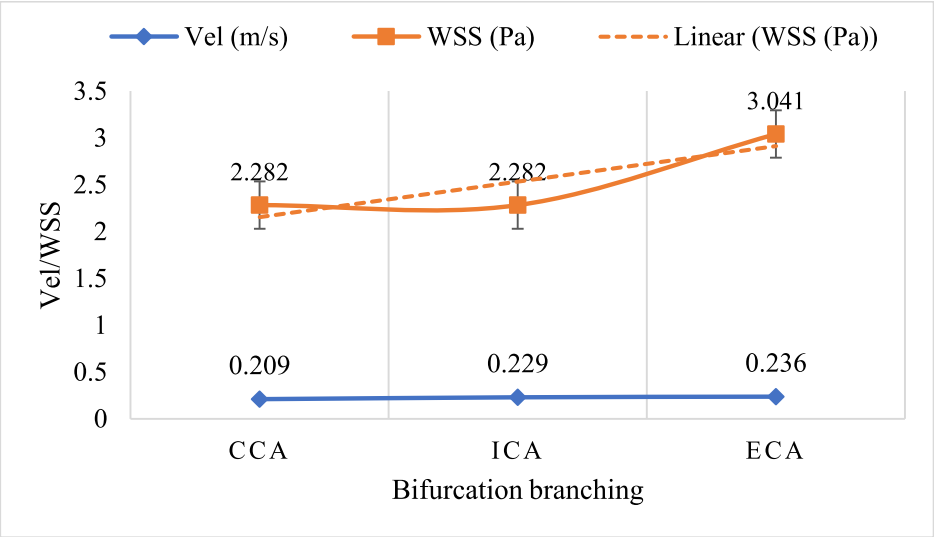

Fig. 13. Flow profile of direct relationship between velocity of flow and corresponding wall shear stress in all branches of the unhealthy carotid artery model (CCA, ICA and ECA) under study.

place at the attaching surfaces for smaller plaque deposits, but the larger plaque exhibits the greatest deformation on the main flow surface. It implies that the nature of displacement and rupture of plaques are influenced by their realistic properties and orientation, which is not often accounted for in most FSI studies. By identifying the regions of the plaque that are most vulnerable to rupture, these findings can inform the development of targeted interventions aimed at reducing the risk of plaque rupture and its associated complications.

- The CFD study shows that the peak WSS in the healthy carotid artery occurs at the bifurcation, with almost no shear stress in the sinus during undisrupted blood flow. However, the FSI simulation reveals minimal shear stress distribution on the arterial walls around the plaque deposits, but significantly high value at the exact region of atherosclerosis, resulting from the drag force on the wall from both the plaque's displacement and forceful blood passage.
- The 85 to 90% lumen reduction by the elastic opposite-end plaques, favored blood supply into the face and neck region with a speed approximately 75% greater than the delivery speed into the brain. Likewise, the forceful flow of blood and displacement of plaques at the narrow passage, pulls ruptured deposits upstream the ICA. Both cases are attributed to ischemia, affecting the brain tissues and eventually leading to stroke.
- Previous FSI studies of plaques in elastic carotid sinus wall, report that blood flow velocity drops at the base of the plaque and is later delivered out of the constriction in a jet-like flow as pressure decreases. However, this current study reveals that there are different unsteady flow patterns at different regions on the deposit, which is influenced by the deposit's orientation and displacement to flow force. This is particularly useful information for further studies of hemodynamic in patient-specific concentric lumen reduction.

Ethical approval

Work on human beings that is submitted to *Medical Engineering & Physics* should comply with the principles laid down in the Declaration of Helsinki; Recommendations guiding physicians in biomedical research involving human subjects. Adopted by the 18th World Medical Assembly, Helsinki, Finland, June 1964, amended by the 29th World Medical Assembly, Tokyo, Japan, October 1975, the 35th World Medical Assembly, Venice, Italy, October 1983, and the 41st World Medical Assembly, Hong Kong, September 1989. You should include information as to whether the work has been approved by the appropriate ethical committees related to the institution(s) in which it was performed and that subjects gave informed consent to the work .

Funding

None.

Declaration of Competing Interest

The authors declare that they have no known competing financial interests or personal relationships that could have appeared to influence the work reported in this paper.

References

[1] Purves D., Augustine G.J., Fitzpatrick D., et al., editors. Neuroscience. 2nd ed. Sunderland (MA): Sinauer Associates; 2001. The Blood Supply of the Brain and Spinal Cord. Available from: https://www.ncbi.nlm.nih.gov/books/NBK11042/.

[2] Hosseini V, Mallone A, Mirkhani N, Noir J, Salek M, Pasqualini FS, et al. A pulsatile flow system to engineer aneurysm and atherosclerosis mimetic extracellular matrix. Adv Sci 2020:2000173.

[3] Goldstein LB, Bushnell CD, Adams RJ, Appel LJ, Braun LT, Chaturvedi S, Creager MA, Culebras A, Eckel RH, Hart RG, Hinchey JA, Howard VJ, Jauch EC, Levine SR, Meschia JF, Moore WS, Nixon JV, Pearson TA. Guidelines for the primary prevention of stroke: a guideline for healthcare professionals from the American heart association. Am Stroke Assoc 2011;42(2):517–84. Feb.

[4] Thanvi B, Robinson T. Complete occlusion of extracranial internal carotid artery: clinical features, pathophysiology, diagnosis and management. Postgrad Med J 2007;83(976):95–9. https://doi.org/10.1136/pgmj.2006.048041. Feb.

[5] Zheng Z, Zhao Q, Wei J, Wang B, Wang H, Meng L, Xin Y, Jiang X. Medical prevention and treatment of radiation-induced carotid injury. Biomed Pharmacother 2020;131:110664. https://doi.org/10.1016/j.biopha.2020.110664. VolumeISSN 0753-3322.

[6] Wijeratne T, Menon R, Sales C, Karimi L, Crewther S. Carotid artery stenosis and inflammatory biomarkers: the role of inflammation-induced immunological responses affecting the vascular systems. Ann Transl Med 2020;8(19):1276. https://doi.org/10.21037/atm-20-4388.

[7] Brinjikji W, Huston J, Rabinstein AA, Kim GM, Lerman A, Lanzino G. Contemporary carotid imaging: from degree of stenosis to plaque vulnerability. J Neurosurg 2016;124(1):27–42. https://doi.org/10.3171/2015.1.JNS142452. Jan.

[8] Kumins NH, King AH, Ambani RN, Thomas JP, Kim AH, Augustin G, Wong VL, Harth KC, Cho JS, Colvard B, Kashyap VS. Anatomic criteria in the selection of treatment modality for atherosclerotic carotid artery disease. J Vas Surg 2020;72(4):1395–404. https://doi.org/10.1016/j.jvs.2020.01.041. VolumeIssuePagesISSN 0741-5214.

[9] Yang Y, Li Z, Liu Q, Guo Y, Mei Y, Lyu J, Zhao M, Feng Y, Xie G. Carotid arterial wall MRI of apolipoprotein e–deficient mouse at 7 T using DANTE-prepared variable-flip-angle rapid acquisition with relaxation enhancement. Magn Reson Imaging 2022;86:1–9. https://doi.org/10.1016/j.mri.2021.10.026. VolumePagesISSN 0730-725X.

[10] Lee SH, Kang S, Hur N, et al. A fluid-structure interaction analysis on hemodynamics in carotid artery based on patient-specific clinical data. J Mech Sci Technol 2012;26:3821–31. https://doi.org/10.1007/s12206-012-1008-0.

[11] Ezzat MA, Lewis RW. Two-dimensional thermo-mechanical fractional responses to biological tissue with rheological properties. Int J Numer Methods Heat Fluid Flow 2022;32(6):1944–60. https://doi.org/10.1108/HFF-03-2021-0201.

[12] Ezzat MA, Alabdulhadi MH. Thermomechanical interactions in viscoelastic skin tissue under different theories. Indian J Phys 2023;97:47–60. https://doi.org/10.1007/s12648-021-02261-4.

[13] Ezzat MA. Thermo-mechanical memory responses in a thick tumorous skin tissue during hyperthermia treatment. Waves Random Complex Media 2021. https://doi.org/10.1080/17455030.2021.2004334.

[14] Adie GA, Fsogbon SK, Ige EO. The effect of ambient air velocity on gaseous aerosol nucleation within a moist lung. In: Proceedings of the International Conference of Mechanical Engineering2. Energy Technology and Management, University of Ibadan; 2016. p. 199–209.

[15] Fasogbon SK, Oyelami FH, Adetimirin EO, Ige EO. On Blasius plate solution of particle dispersion and deposition in human respiratory track. Math Model Eng Prob 2019;6(3):428–32. https://doi.org/10.18280/mmep.060314.

[16] O.yejide AJ, Emmanuel E, Awonusi AA, I.ge EO. A Computational study of respiratory biomechanics in idealized healthy and stenosed subsegmental bronchi section of infant, child and adult airways. Ser Biomech 2022;36(4):25–45. https://doi.org/10.7546/SB.04.04.2022.

[17] James Ayodele O, Oluwatosin AE, Taiwo OC, Dare AA. Computational fluid dynamics modeling in respiratory airways obstruction: current applications and prospects. Int J Biomed Sci Eng 2021;9(2):21–31. https://doi.org/10.11648/j.ijbse.20210902.12. Vol.

[18] Pillai GM, Jayakumar JS, Kumar RA, Mahanta P, Kalita P, Paul A, Banerjee A. Fluid–structure interaction analysis in an atherosclerosis carotid artery. Advances in thermofluids and renewable energy. Lecture notes in mechanical engineering. Singapore: Springer; 2022. https://doi.org/10.1007/978-981-16-3497-0_2.

[19] Moradicheghamahi J, Jahangiri M, Mousaviraad M, et al. Computational studies of comparative and cumulative effects of turbulence, fluid–structure interactions, and uniform magnetic fields on pulsatile non-Newtonian flow in a patient-specific carotid artery. J Braz Soc Mech Sci Eng 2020;42:518. https://doi.org/10.1007/s40430-020-02608-8.

[20] Oyejide AJ, et al. Simulation of inspiratory airflow in stenotic trachea and its effect on mainstem bifurcation. Saudi J Biomed Res 2021;6(11):256–63. https://doi.org/10.36348/sjbr.2021.v06i11.002.

[21] Nagargoje M, Gupta R. Effect of sinus size and position on hemodynamics during pulsatile flow in a carotid artery bifurcation. Comput Methods Progr Biomed 2020;192:105440. https://doi.org/10.1016/j.cmpb.2020.105440. VolumeISSN 0169-2607.

[22] Ayodele OJ, Taiwo OC, Ayoade AA. Numerical simulations of inlet and outlet air flow dynamics in healthy and stenosis adult airway. J Adv Res Appl Mech Compu Fluid Dyna 2021;8(3&4):1–7. https://doi.org/10.24321/2349.7661.202102.

[23] Sia SF, Zhao X, Li R, Zhang Y, Chong W, He L, Chen Y. Evaluation of the carotid artery stenosis based on minimization of mechanical energy loss of the blood flow. Proc Inst Mech Eng Part H J Eng Med 2016;230(11):1051–8. https://doi.org/10.1177/0954411916671752.

[24] Chiastra C, Migliavacca F, Martínez MÁ, Malvè M. On the necessity of modelling fluid–structure interaction for stented coronary arteries. J Mech Behav Biomed Mater 2014;34:217–30. https://doi.org/10.1016/j.jmbbm.2014.02.009. VolumePagesISSN 1751-6161.

[25] Albufeira/Portugal 11-15 June 2017Editors Sousa1 LC, Castro1 CF, António1 CC, Azevedo E, Silva Gomes JF, Meguid SA. In: Proceedings of the 7th international conference on mechanics and materials in design; 2017. Albufeira/Portugal 11-15 June 2017EditorsPubl. INEGI/FEUP.

[26] Zouggari L, Bou-said B, Massi F, Culla A, Millon A. The role of biomechanics in the assessment of carotid atherosclerosis severity: a numerical approach. World J Vasc Surg 2018;1(1):1007.
[27] Lopes D, Puga H, Teixeira JC, Teixeira SF. Influence of arterial mechanical properties on carotid blood flow: comparison of CFD and FSI studies. Int J Mech Sci 2019. https://doi.org/10.1016/j.ijmecsci.2019.06.029.
[28] Bantwal A, Singh A, Menon AR, Kumar N. Pathogenesis of atherosclerosis and its influence on local hemodynamics: a comparative FSI study in healthy and mildly stenosed carotid arteries. Int J Eng Sci 2021;167:103525. https://doi.org/10.1016/j.ijengsci.2021.103525. VolumeISSN 0020-7225.
[29] Cunnane EM, Mulvihill JJ, Barrett HE, Walsh MT. Simulation of human atherosclerotic femoral plaque tissue: the influence of plaque material model on numerical results. Biomed Eng Online 2015;14(1):S7. https://doi.org/10.1186/1475-925X-14-S1-S7. Suppl 1Suppl.
[30] Rahdert DA, Sweet WL, Tio FO, Janicki C, Duggan DM. Measurement of density and calcium in human atherosclerotic plaque and implications for arterial brachytherapy. Cardiovasc Radiat Med 1999;1(4):358–67. https://doi.org/10.1016/s1522-1865(00)00030-5.
[31] Rabbi MF, Laboni FS, Tarik Arafat M. Computational analysis of the coronary artery hemodynamics with different anatomical variations. Inform Med Unlocked 2020;19:100314. https://doi.org/10.1016/j.imu.2020.100314. Volume2020ISSN 2352 9148.
[32] Sinnott M, Cleary PW, Prakash M. An investigation of pulsatile blood flow in a bifurcation artery using a grid-free method. In: Proceedings of the 5th international conference CFD process industry; 2006. p. 1–6.
[33] Morbiducci U, Gallo D, Massai D, Ponzini R, Deriu MA, Antiga L, Redaelli A, Montevecchi FM. On the importance of blood rheology for bulk flow in hemodynamic models of the carotid bifurcation. J Biomech 2011;44(13):2427–38. https://doi.org/10.1016/j.jbiomech.2011.06.028. VolumeIssuePagesISSN 0021-9290.
[34] edited by Carvalho V, Bhattacharyya S, et al. Comparison of CFD and FSI simulations of blood flow in stenotic coronary arteries. Computational fluid dynamics [Working title]. IntechOpen; 2022. https://doi.org/10.5772/intechopen.102089. edited by.
[35] Mohammadian SK, Zhang Y. Thermal management optimization of an air-cooled Li-ion battery module using pin-fin heat sinks for hybrid electric vehicles. J Power Sources 2014;273:431–9. https://doi.org/10.1016/j.jpowsour.2014.09.110.
[36] Oyewola OM, Awonusi AA, Ismail OS. Performance improvement of air-cooled battery thermal management system using sink of different pin-fin shapes. Emerg Sci J 2022;6(4):851–65. https://doi.org/10.28991/ESJ-2022-06-04-013.
[37] Tomaszewski M, Baranowski P, Malachowski J, Damaziak K, Bukała J. Analysis of artery blood flow before and after angioplasty. AIP Conf Proc 2018;1922:070001. https://doi.org/10.1063/1.5019068.
[38] Wolters FJ, Zonneveld HI, Hofman A, Lugt A, Koudstaal PJ, Vernooij MW, Arfan Ikram M. Cerebral perfusion and the risk of dementia. Circulation 2017;136(8):719–28. https://doi.org/10.1161/CIRCULATIONAHA.117.027448.
[39] Leeuwis AE, Smith LA, Melbourne A, Hughes AD, Richards M, Prins ND, Sokolska M, Atkinson D, Tillin T, Jäger HR, Chaturvedi N, van der Flier WM, Barkhof F. Cerebral blood flow and cognitive functioning in a community-based, multi-ethnic cohort: the sabre study. Front Aging Neurosci 2018;10:279. https://doi.org/10.3389/fnagi.2018.00279.
[40] Xing, R., 2019. Wall shear stress and atherosclerotic plaque progression.
[41] Badimon L, Vilahur G. Thrombosis formation on atherosclerotic lesions and plaque rupture. J Internal Med 2014;276(6):618–32.
[42] Rognoni A, Cavallino C, Veia A, Bacchini S, Rosso R, Facchini M, G Secco G, Lupi A, Nardi F, Rametta F, S Bongo A. Pathophysiology of atherosclerotic plaque development. Cardiovasc Hematol Agents Med Chem 2015;13(1):10–3 (Formerly Current Medicinal Chemistry-Cardiovascular & Hematological Agents).
[43] Gaba P, Gersh BJ, Muller J, Narula J, Stone GW. Evolving concepts of the vulnerable atherosclerotic plaque and the vulnerable patient: implications for patient care and future research. Nat Rev Cardiol 2023;20(3):181–96.